Electronic Supplementary Information

A Recirculation System for Concentrating CO_2 Electrolyzer Products

Tobias A. Kistler[1,2], Rajiv R. Prabhakar[1,2], Peter Agbo[1,2,*]

[1]Chemical Sciences Division, Lawrence Berkeley National Laboratory, Berkeley, California 94720, USA

[2]Liquid Sunlight Alliance, Lawrence Berkeley National Laboratory, Berkeley, California 94720, USA

[*]Corresponding Author: pagbo@lbl.gov

Ethylene outlet concentrations reported in literature

Since the ethylene concentration ($c_{c_2H_4}$) was not reported for most publications found in the existing literature, it was calculated from published data using the faradaic efficiency (*FE*), current (*I*) and volumetric flow rate ($\dot{V}$) at standard conditions:

$$c_{c_2H_4} = \frac{FE * \mathrm{R} * \mathrm{T} * I}{\mathrm{p} * \dot{V} * \mathrm{n_{e^-}} * \mathrm{F}}, \quad (1)$$

with R as the gas constant (8.3145 J K^{-1} mol^{-1}), T and p as the temperature (298.15 K) and pressure (1.01325*10^5 Pa) at standard conditions, respectively, n_{e^-} as the number of electrons (12) transferred per molecule of ethylene generated and F as the Faraday constant (96485.33 C mol^{-1}). The calculated values for $c_{c_2H_4}$ are shown in **Table S1**. The publications from Gabardo *et al.*[1] and Ozden *et al.*[2] report the concentrations for ethylene which are displayed in parentheses in **Table S1**. Discrepancies between the directly reported and calculated values could be explained by differing inlet and outlet cathode flow rates. For calculations using equation (1), only the inlet flow rate could be considered since the outlet flow rate was not reported, but ideally the outlet flow rate is used for accurate concentration calculations.

Table S1 Ethylene concentrations for notable devices reported to date, calculated from published faradaic efficiency, current density (*j*), area (*A*) and flow rate values. Concentration values in parentheses were taken directly from the published reports.

Reference	FE	j [A cm^{-2}]	$j_{c_2H_4}$ [A cm^{-2}]	A [cm^2]	I [A]	$\dot{V}$ [sccm]	$c_{c_2H_4}$ [%]
Gabardo *et al.*[1]	0.48	0.05	0.02	5	0.25	3	5.07 (30)
Ozden *et al.*[2]	0.28	0.30	0.08	5	1.50	3	17.75 (37)
Xu *et al.*[3]	0.42	0.50	0.21	0.5	0.25	20	0.67
Wang *et al.*[4]	0.46	0.80	0.37	2	1.60	20	4.67
Liu *et al.*[5]	0.71	0.25	0.18	4.5	1.13	20	5.07
Li *et al.*[6]	0.64	0.34	0.22	5	1.68	20	6.82
Lin *et al.*[7]	0.40	0.15	0.06	3.25	0.49	50	0.49
Wang *et al.*[8]	0.70	0.50	0.35	1	0.50	50	0.89
Li *et al.*[9]	0.64	0.12	0.08	5	0.60	50	0.97
Ma *et al.*[10]	0.65	1.60	1.04	1	1.60	50	2.64
Nam *et al.*[11]	0.49	1.00	0.49	5	5.00	50	6.23
Zhong *et al.*[12]	0.80	0.40	0.32	1	0.40	56	0.72
Lee *et al.*[13]	0.55	0.28	0.15	10	2.80	100	1.93
Merino-Garcia *et al.*[14]	0.91	0.01	0.01	10	0.08	180	0.05

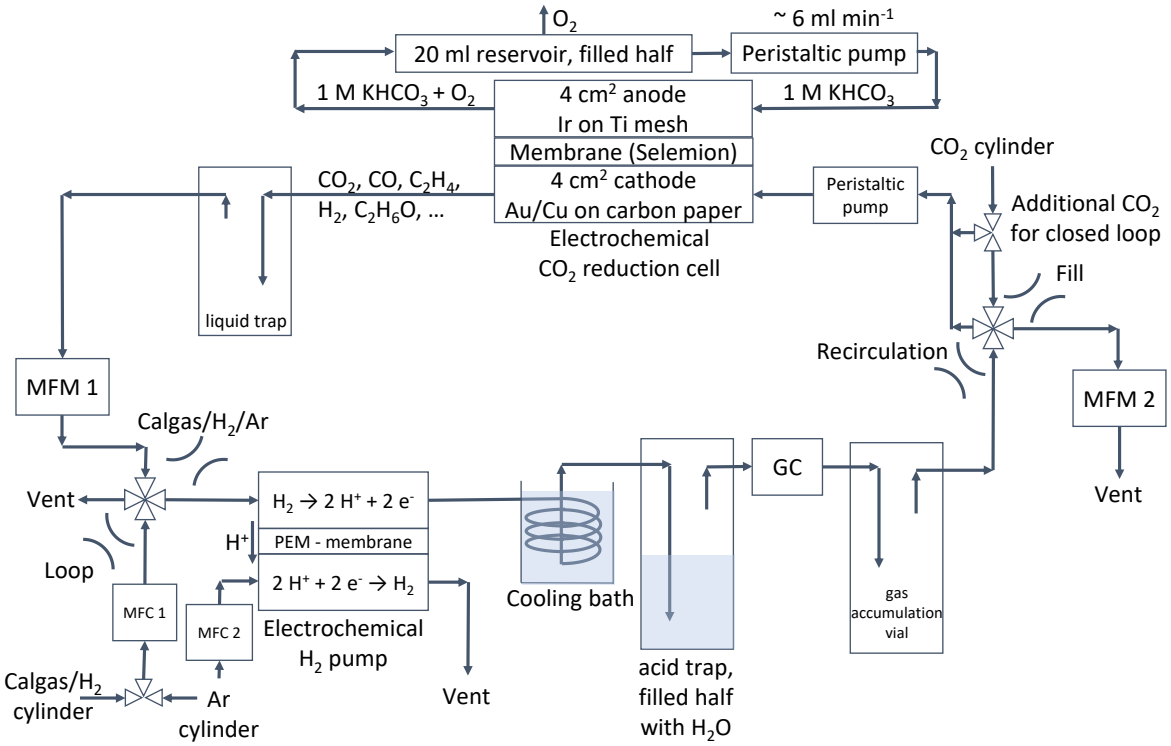

(a)

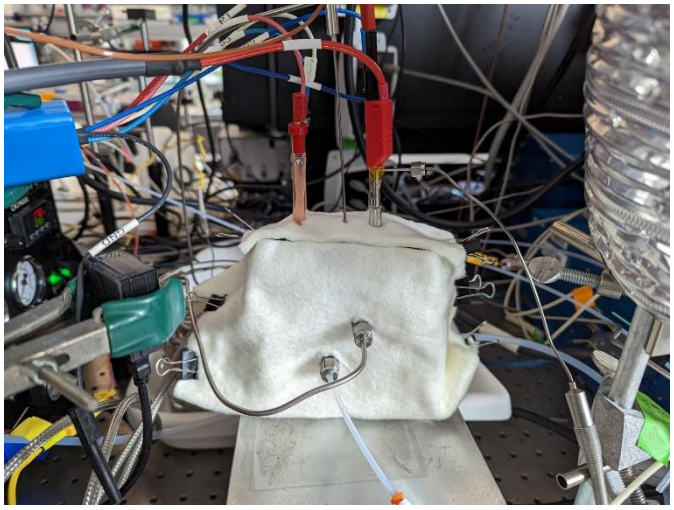

(b)

Fig. S1 Full gas recycling system (a) shown in a simplified manner in **Fig. 2** of the main manuscript. A trap was installed behind the cathode outlet to collect any liquid products from the CO_2 reduction cell. A mass flow meter (MFM) was measuring the flowrate and pressure inside of the loop and another MFM was installed at the end of the loop to check for leaks. The 4-way valve installed before the H_2 pump's anode inlet enabled switching between CO_2

reduction cell outlet and pure H_2/Ar feed. Mass flow controllers (MFCs) were used to control the H_2 and Ar flow rates going into the H_2 pump. Since the H_2 pump was operated at elevated temperatures, a cooling bath consisting of coiled stainless steel tubing immersed in water was positioned behind the H_2 pump outlet. A water-filled acid trap collected any phosphoric acid which could have leached out of the membrane from the H_2 pump. The gas accumulation vial behind the gas chromatograph (GC) enabled mixing of gas ejected from the GC during valve switches with the product stream, which stabilized the pressure and provided more stable cell performance. (b) An image of the heat-insulated electrochemical H_2 pump used for H_2 removal in the recirculator.

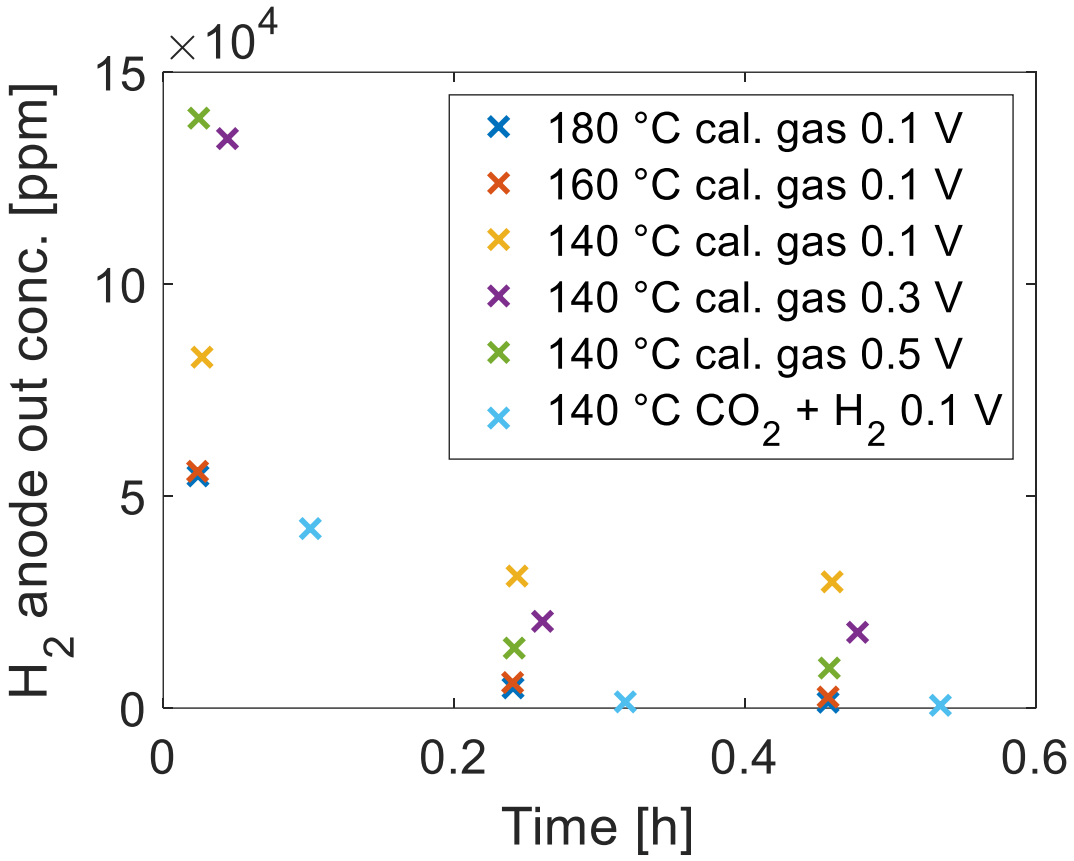

Fig. S2 Hydrogen anode outlet concentrations during operation of the H_2 pump with CO-containing calibration gas at different temperatures and voltages. Under conditions of CO poisoning (140 °C), H_2 is detected at the anode outlet even after 30 min of operation, indicating that not all of the incoming H_2 is converted to protons and pumped across the membrane.

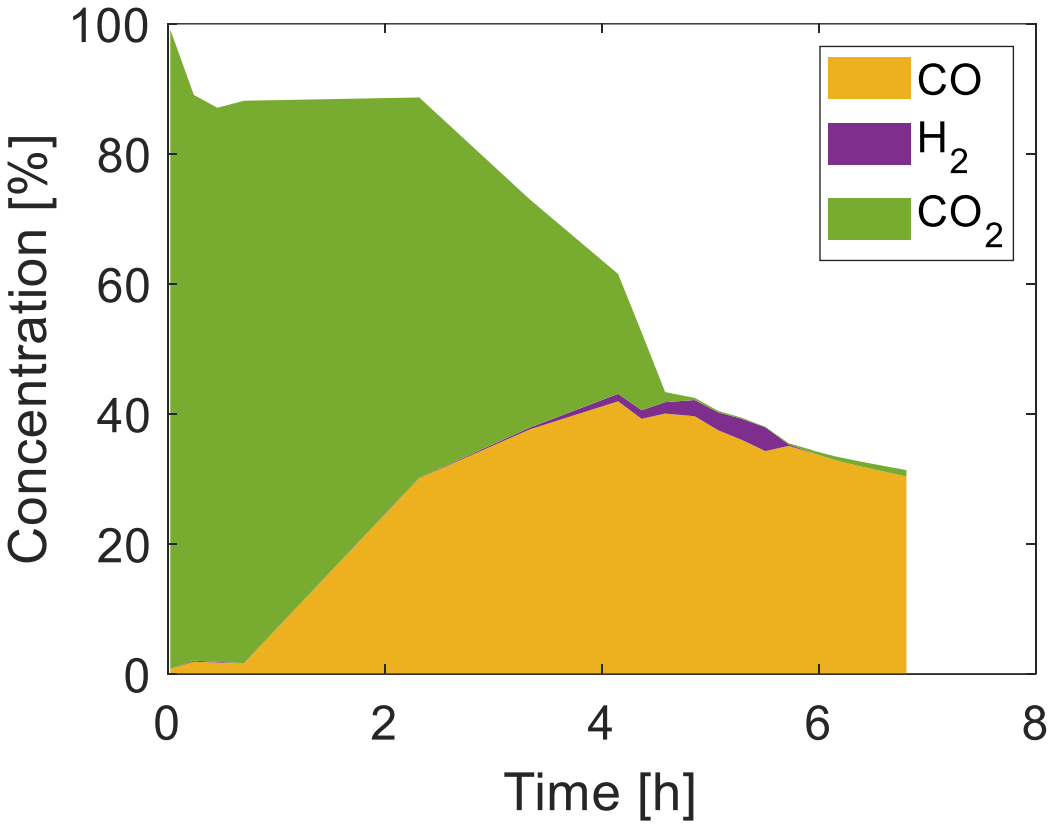

Fig. S3 Recirculation experiment performed with Au as the CO_2 reduction catalyst. The CO concentration rises steadily while H_2 is removed by the H_2 pump. Towards the end of the experiment, a large fraction of gases is unaccounted for since GC carrier gas, which cannot be quantified by the GC, is injected into the gas recirculation loop after every GC valve switch cycle.

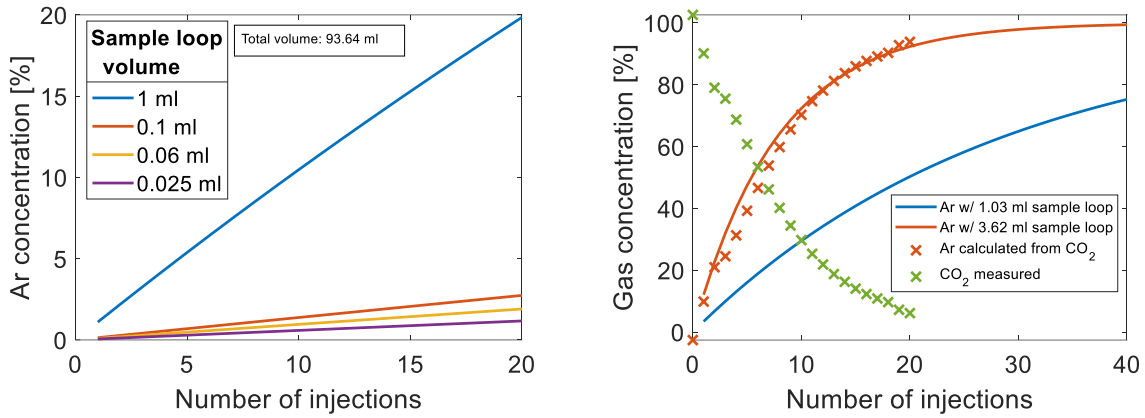

(a) (b)

Fig. S4 GC carrier gas (Ar) concentration in the recirculation loop as a function of GC injections. (a) With a smaller sample loop, the amount of injected carrier gas is lower. Results are shown for a total gas loop volume of 93.64 ml. (b) Measured CO_2 concentration as a function of GC injections (green crosses). With every GC injection, the concentration of CO_2 drops since some CO_2 is replaced with argon after each GC valve cycle. Here, the concentration of Ar was estimated by subtracting the concentration of CO_2 from 100%. It becomes evident that the estimated amount of Ar (red crosses) does not match the calculation (blue line) considering a sample loop size of 1.03 ml, the actual size of the installed GC sample loop. However, the estimated amount of Ar matches rather well with a 3.62 ml sized sample loop. Due to the fact that the GC carrier gas is pressurized, the amount of carrier gas injected into the gas recirculation loop is increased by a factor of ~3 compared to an unpressurized sample loop. This results in a much larger effect of the carrier gas on the recirculation system performance than initially expected. Results shown are for a simpler gas recirculation system without electrochemical cells and a total gas loop volume of ~30 ml.

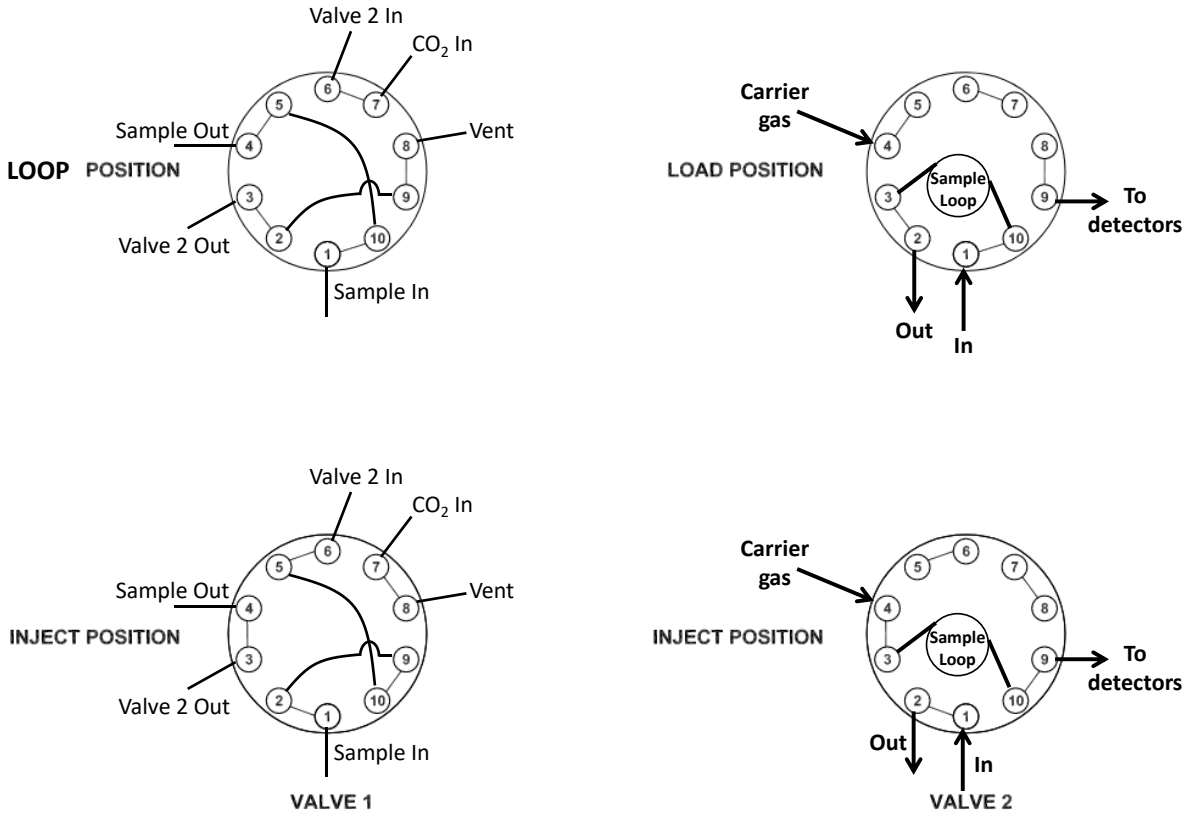

Fig. S5 Modified GC valve system. In the LOOP position, the product stream simply enters valve 1 and exits. During a gas recirculation experiment, valve 1 is first switched to the INJECT position, allowing the product stream to flow through valve 2, which is initially kept in LOAD position. This switch of valve 1 effectively injects a small amount of CO_2, which is flowing through valve 2 and the sample loop while valve 1 is in LOOP position, into the gas recirculation loop. After 3 minutes, the sample loop installed on valve 2 is sufficiently flushed with the product stream and the sample can be injected onto the GC columns and detectors (INJECT position of valve 2). Shortly after, valve 1 is switched back to the LOOP position, shielding the gas recirculation loop from any GC carrier gas influence. When valve 2 is switched back to the LOAD position at the end of the GC cycle, the pressurized carrier gas in the sample loop is vented through port 8 of valve 1, instead of being injected into the gas recirculation loop. It should be noted that valve 2 is shown in a simplified manner.

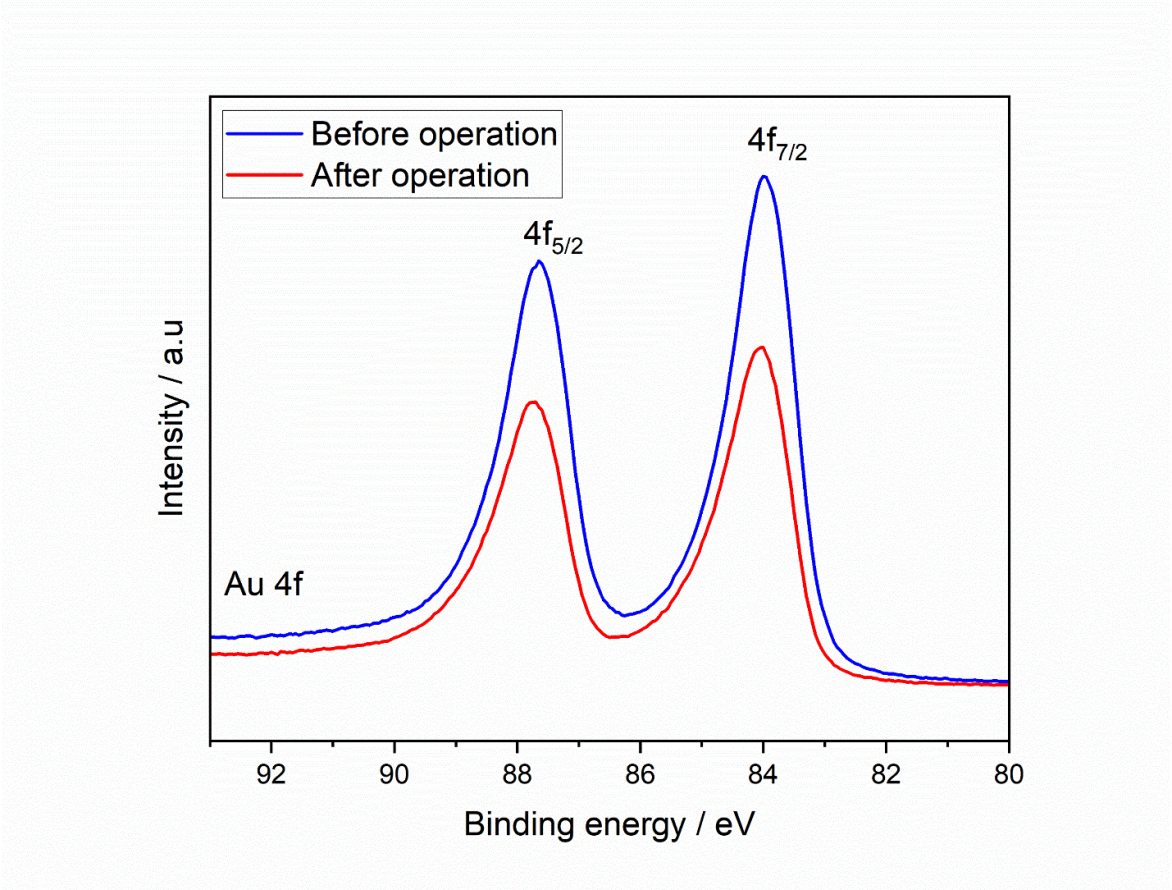

Fig. S6 XPS core level spectra for Au 4f of Au electrocatalysts deposited on AvCarb substrate via RF sputtering as described in Materials and Methods. Data shown represent the Au catalyst before and after 8.5 hours of CO_2 electrolysis performed at 3 V cell bias (see **Fig. 4** in the main manuscript). Data show no significant change in Au catalyst composition as a function of device turnover; reduction in overall Au 4f signal intensities are assigned to moderate delamination of Au from the AvCarb substrate following device dismantling after the experiment.

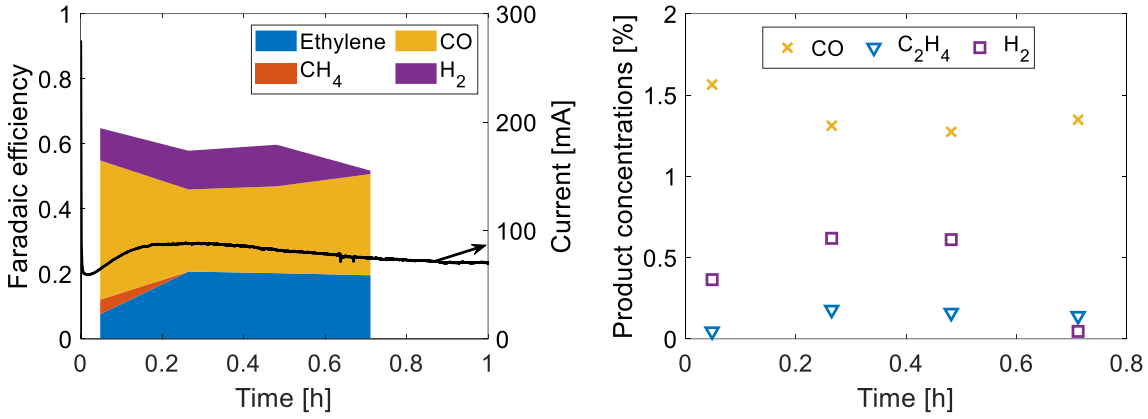

(a) (b)

Fig. S7 Single-pass experiment performed with Cu as the CO_2 reduction catalyst, operated at 4 V at a cathode flow rate of ~13 sccm. (a) Faradaic efficiency of ~20% for C_2H_4. (b) Product concentrations over time, showing a peak C_2H_4 concentration of ~0.2%. At a cathode flow rate of ~7 sccm, which is roughly half of the tested flow rate, the generated C_2H_4 concentration can be projected to be doubled, yielding a value around 0.4%. It should be noted, that this assumes that the selectivity does not change significantly by going from 13 to 7 sccm.

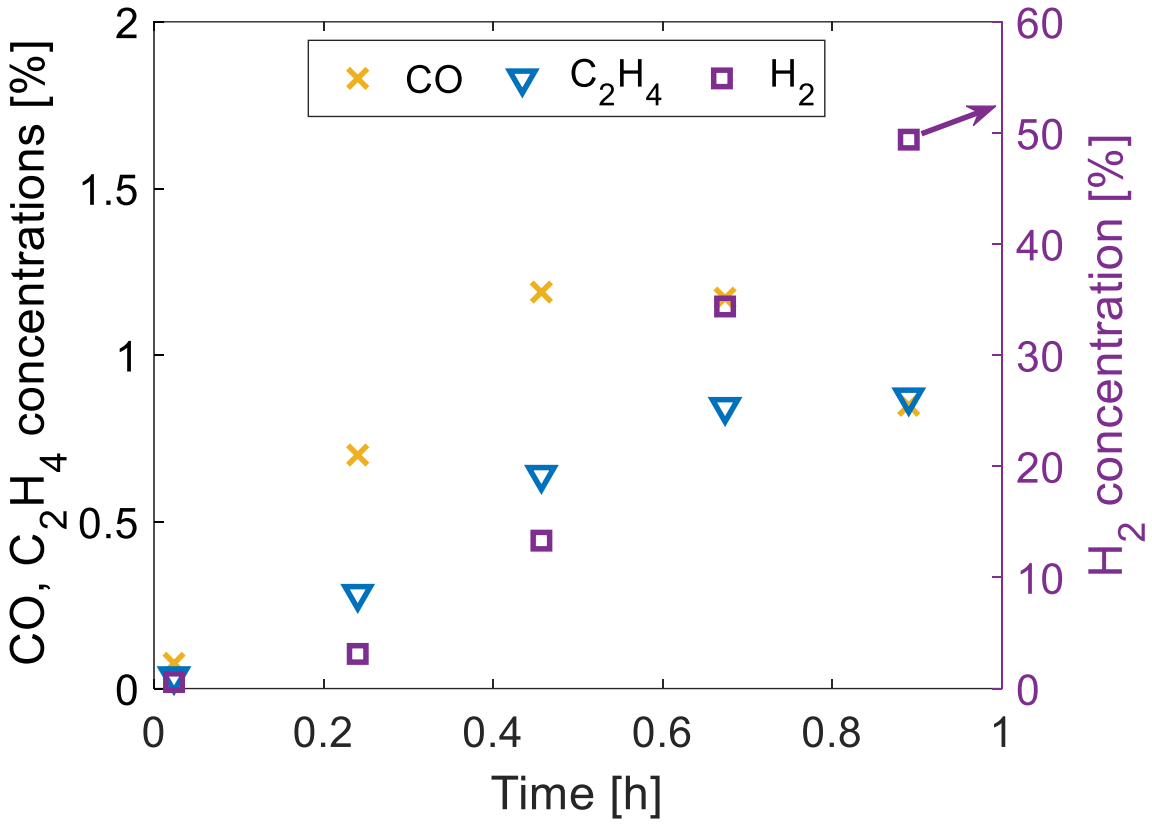

Fig. S8 Recirculation experiment performed with Cu as the CO_2 reduction catalyst, operated at 4 V and without H_2 pump. H_2 quickly accumulated and prevented further generation of C_2H_4.

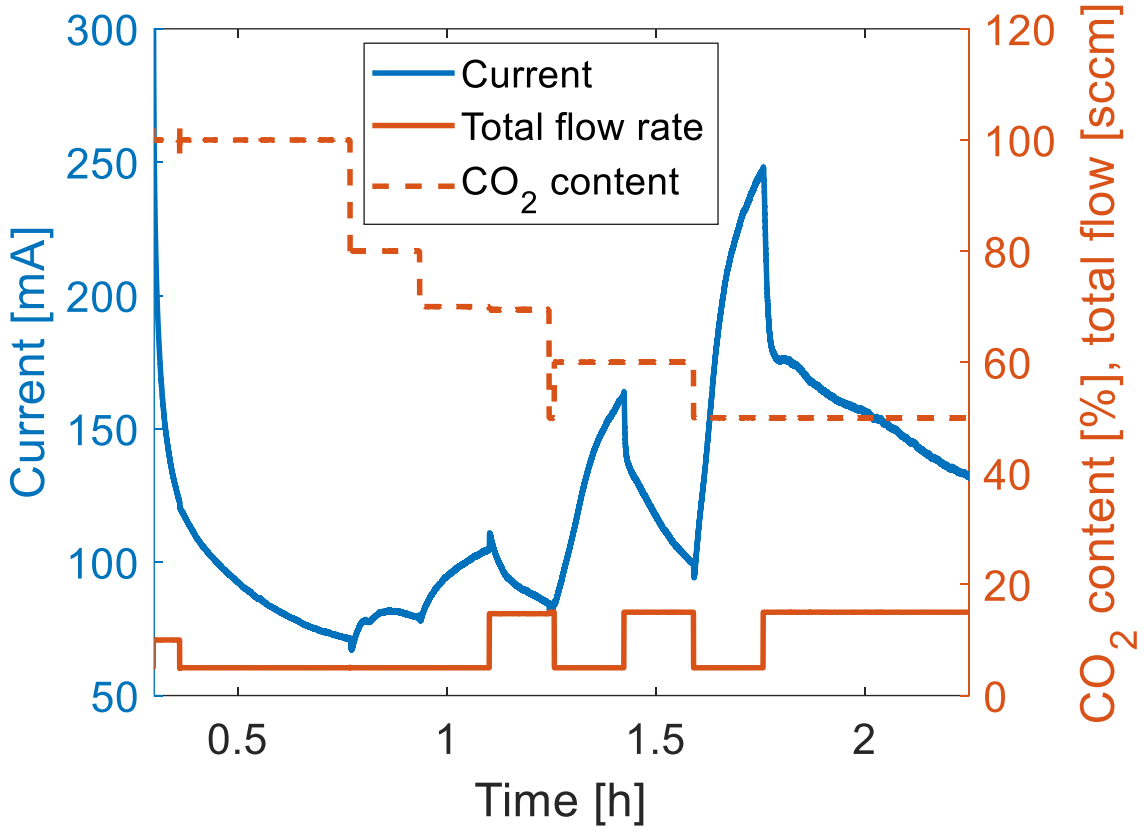

Fig. S9 Single-pass experiment performed with Cu as the CO_2 reduction catalyst, operated at 4 V. The flow rate was cycled between 5 and 15 sccm, and the concentration of CO_2 steadily dropped from 100% to 50% by diluting the CO_2 inlet flow with Ar. As the concentration of CO_2 dropped, the current immediately spiked up even at fairly high CO_2 concentrations of 80%, indicating vastly increased hydrogen evolution reaction (HER) rates with larger spikes at lower CO_2 contents. The spikes were reversible by increasing the total inlet flow rate, indicating that, at reduced CO_2 concentrations, both the CO_2 concentration and the CO_2 mass flow rate influence the selectivity between CO_2 reduction and HER, with the latter dominating at conditions of low CO_2 availability. Therefore, it can be expected that a minimum flow rate exists for a certain cell architecture and set of operating conditions, which maximizes the concentrations of CO_2 reduction products leaving the electrolyzer but prevents HER from dominating.

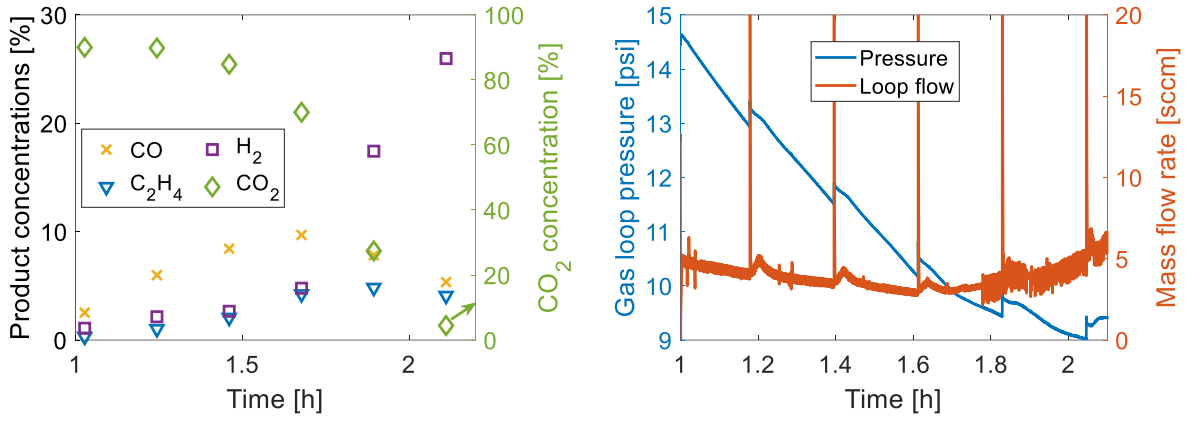

(a) (b)

Fig. S10 Recirculation experiment performed with Cu as the CO_2 reduction catalyst, operated at 4 V. The system was first operated in single-pass mode for 1 h, after which the gas loop was closed. No fresh CO_2 was supplied while the loop was closed (1 h – 2.25 h). (a) Product and CO_2 concentrations over time, indicating a peak C_2H_4 concentration of 4.8%. It should be noted that the GC was installed before the H_2 pump for this test, explaining the higher measured H_2 concentrations. (b) Pressure and mass flow rate in the gas loop. Since no CO_2 was added to the closed loop, the pressure dropped quickly over time.

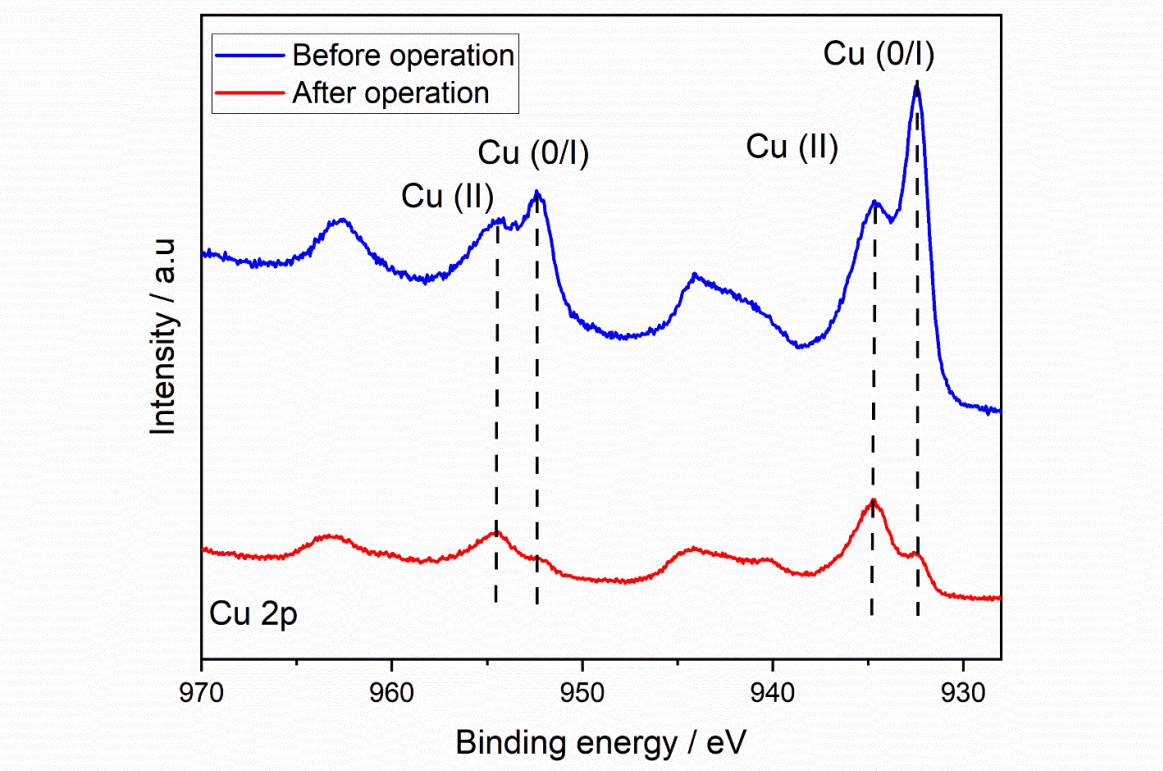

Fig. S11 XPS core level spectra for Cu 2p of Cu electrocatalysts deposited on AvCarb substrate via radio frequency (RF) sputtering as described in Materials and Methods, before and after 6 hours of recirculated CO_2 electrolysis at 4 V (see **Fig. 5** in the main manuscript). XPS was employed to probe the oxidation states of the Cu catalyst before and after CO_2R operation as described in the manuscript. Catalytic turnover of metallic Cu in the cathode gas diffusion electrode is shown to result in a decreased peak intensity of the characteristic peak for the Cu (0/I) oxidation state.[15] In addition, the relative intensities of the Cu (0/I) and Cu (II) 2p core levels are shown to switch during operation, with Cu (II) signals becoming more prominent after CO_2R operation.

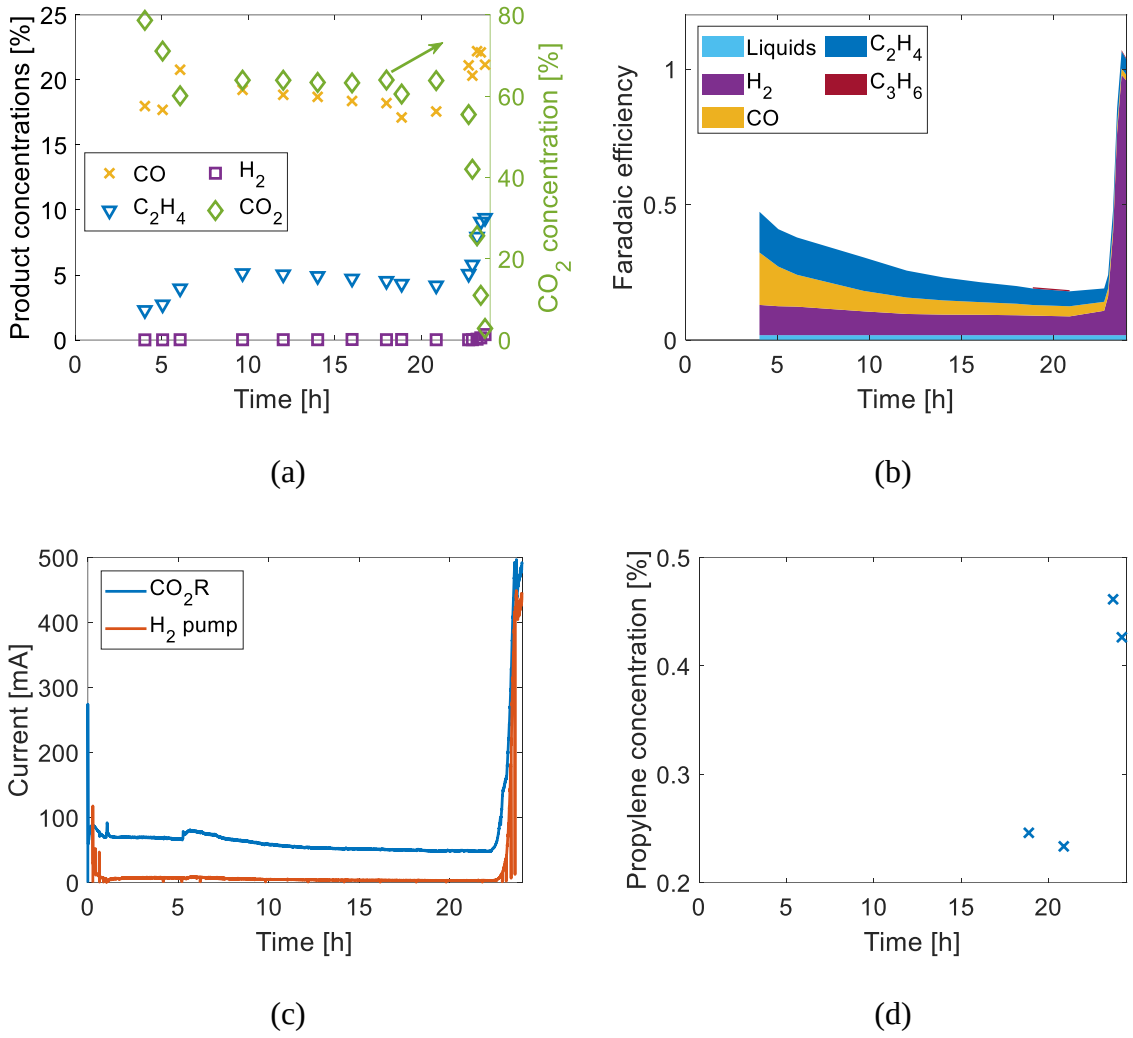

Fig. S12 Long-term recirculation experiment performed with Cu as the CO_2 reduction catalyst, operated at 4 V. (a) Product concentrations over time, showing a peak C_2H_4 concentration of 9.4%. Since the recirculation flow rate was ~7 sccm, this marks a ~20-fold improvement over the single-pass test shown in **Fig. S7**. (b) The faradaic efficiencies of gas products dropped over time due to a suspected gas leak. Liquid products in the anolyte were only quantified after the experiment, with the main detected product being acetate. The faradaic efficiency for H_2 was calculated based on the measured concentration in the loop and the amount of H_2 pumped across the membrane in the H_2 pump. (c) Currents of the CO_2 reduction (CO_2R) cell and H_2 pump, which were used to quantify the faradaic efficiency for H_2. (d) Propylene concentrations near 0.5% were detected towards the end of the experiment.

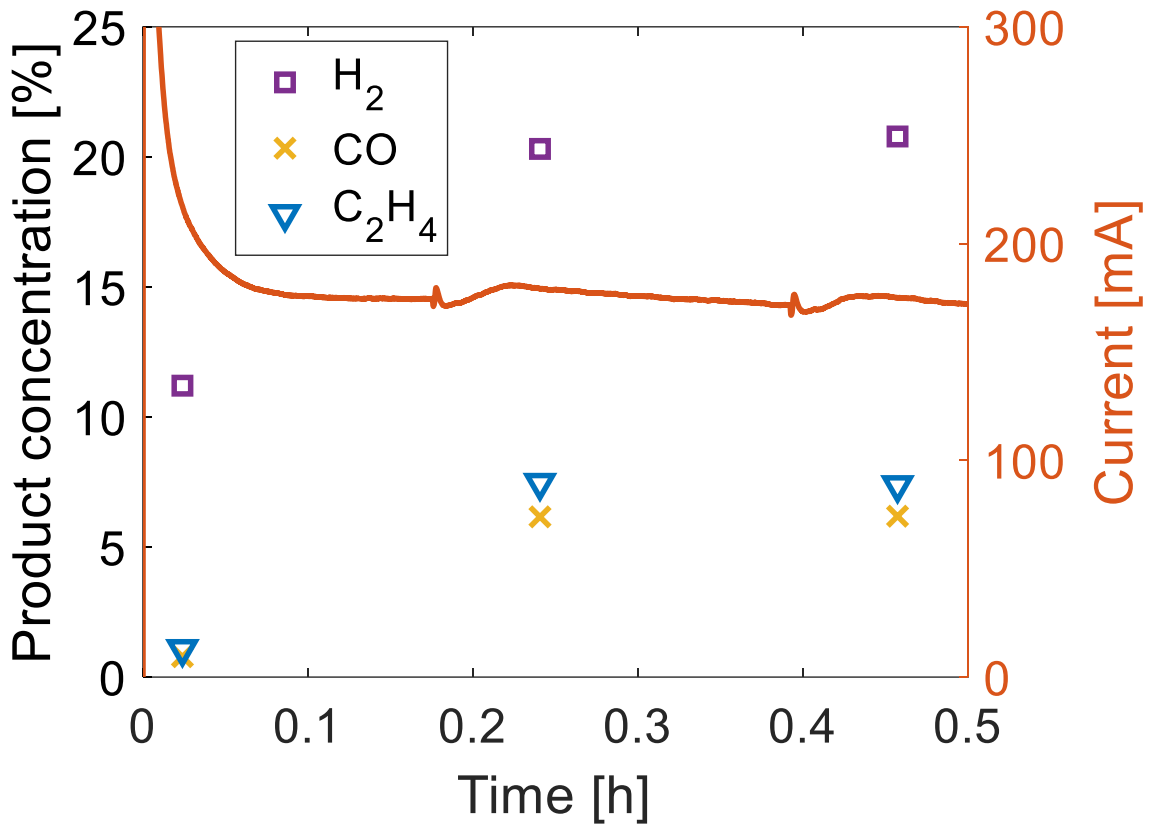

Fig. S13 Single-pass experiment performed with Cu as the CO_2 reduction catalyst, operated at 4 V. A peak C_2H_4 concentration of 7.5% was measured while H_2 concentrations exceeded 20%. The inlet CO_2 flow rate was 2.3 sccm for this test, which resulted in an outlet flow rate of ~0.8 sccm due to CO_2 crossover through the membrane of the CO_2 reduction cell. Reducing the flow rate any further just lead to dominating HER, lowering the produced C_2H_4 concentrations. Due to the already high rates of HER, the overall device current was comparatively higher than during the experiments shown in **Fig. S7** and **Fig. S12**.

References

1 C. M. Gabardo, C. P. O'Brien, J. P. Edwards, C. McCallum, Y. Xu, C.-T. Dinh, J. Li, E. H. Sargent and D. Sinton, *Joule*, 2019, **3**, 2777–2791.

2 A. Ozden, F. Li, F. P. García de Arquer, A. Rosas-Hernández, A. Thevenon, Y. Wang, S.-F. Hung, X. Wang, B. Chen, J. Li, J. Wicks, M. Luo, Z. Wang, T. Agapie, J. C. Peters, E. H. Sargent and D. Sinton, *ACS Energy Lett.*, 2020, **5**, 2811–2818.

3 Y. N. Xu, W. Li, H. Q. Fu, X. Y. Zhang, J. Y. Zhao, X. Wu, H. Y. Yuan, M. Zhu, S. Dai, P. F. Liu and H. G. Yang, *Angewandte Chemie*, 2023, **135**.

4 R. Wang, J. Liu, Q. Huang, L.-Z. Dong, S.-L. Li and Y.-Q. Lan, *Angewandte Chemie (International ed. in English)*, 2021, **60**, 19829–19835.

5 W. Liu, P. Zhai, A. Li, B. Wei, K. Si, Y. Wei, X. Wang, G. Zhu, Q. Chen, X. Gu, R. Zhang, W. Zhou and Y. Gong, *Nature communications*, 2022, **13**, 1877.

6 J. Li, A. Ozden, M. Wan, Y. Hu, F. Li, Y. Wang, R. R. Zamani, D. Ren, Z. Wang, Y. Xu, D.-H. Nam, J. Wicks, B. Chen, X. Wang, M. Luo, M. Graetzel, F. Che, E. H. Sargent and D. Sinton, *Nature communications*, 2021, **12**, 2808.

7 Y.-R. Lin, D. U. Lee, S. Tan, D. M. Koshy, T. Y. Lin, L. Wang, D. Corral, J. E. Avilés Acosta, J. A. Zamora Zeledon, V. A. Beck, S. E. Baker, E. B. Duoss, C. Hahn and T. F. Jaramillo, *Adv Funct Materials*, 2022, **32**.

8 Z. Wang, Y. Li, X. Zhao, S. Chen, Q. Nian, X. Luo, J. Fan, D. Ruan, B.-Q. Xiong and X. Ren, *Journal of the American Chemical Society*, 2023, **145**, 6339–6348.

9 F. Li, A. Thevenon, A. Rosas-Hernández, Z. Wang, Y. Li, C. M. Gabardo, A. Ozden, C. T. Dinh, J. Li, Y. Wang, J. P. Edwards, Y. Xu, C. McCallum, L. Tao, Z.-Q. Liang, M. Luo, X. Wang, H. Li, C. P. O'Brien, C.-S. Tan, D.-H. Nam, R. Quintero-Bermudez, T.-T. Zhuang, Y. C. Li, Z. Han, R. D. Britt, D. Sinton, T. Agapie, J. C. Peters and E. H. Sargent, *Nature*, 2020, **577**, 509–513.

10 W. Ma, S. Xie, T. Liu, Q. Fan, J. Ye, F. Sun, Z. Jiang, Q. Zhang, J. Cheng and Y. Wang, *Nat Catal*, 2020, **3**, 478–487.

11 D.-H. Nam, O. Shekhah, A. Ozden, C. McCallum, F. Li, X. Wang, Y. Lum, T. Lee, J. Li, J. Wicks, A. Johnston, D. Sinton, M. Eddaoudi and E. H. Sargent, *Advanced materials (Deerfield Beach, Fla.)*, 2022, **34**, e2207088.

12 M. Zhong, K. Tran, Y. Min, C. Wang, Z. Wang, C.-T. Dinh, P. de Luna, Z. Yu, A. S. Rasouli, P. Brodersen, S. Sun, O. Voznyy, C.-S. Tan, M. Askerka, F. Che, M. Liu, A. Seifitokaldani, Y. Pang, S.-C. Lo, A. Ip, Z. Ulissi and E. H. Sargent, *Nature*, 2020, **581**, 178–183.

13 W. H. Lee, C. Lim, S. Y. Lee, K. H. Chae, C. H. Choi, U. Lee, B. K. Min, Y. J. Hwang and H.-S. Oh, *Nano Energy*, 2021, **84**, 105859.

14 I. Merino-Garcia, J. Albo, J. Solla-Gullón, V. Montiel and A. Irabien, *Journal of CO2 Utilization*, 2019, **31**, 135–142.

15 X. Cao, S. Ren, X. Zhang, Q. Fan, Q. Chen, J. Yang and J. Mao, *Chem*, 2024, DOI: 10.1016/j.chempr.2024.02.014.